NJC

Accepted Manuscript

This is an *Accepted Manuscript*, which has been through the Royal Society of Chemistry peer review process and has been accepted for publication.

Accepted Manuscripts are published online shortly after acceptance, before technical editing, formatting and proof reading. Using this free service, authors can make their results available to the community, in citable form, before we publish the edited article. We will replace this *Accepted Manuscript* with the edited and formatted *Advance Article* as soon as it is available.

You can find more information about *Accepted Manuscripts* in the Information for Authors.

Please note that technical editing may introduce minor changes to the text and/or graphics, which may alter content. The journal's standard Terms & Conditions and the Ethical guidelines still apply. In no event shall the Royal Society of Chemistry be held responsible for any errors or omissions in this *Accepted Manuscript* or any consequences arising from the use of any information it contains.

ROYAL SOCIETY OF CHEMISTRY

www.rsc.org/njc

Computational Mechanistic Study on pH-Dependent Alcohol Dehydrogenation Catalyzed by A Novel [C, N] or [C, C] Cyclometalated Cp*Ir Complex in Aqueous Solution

Dan-Dan Zhang[a], *Xian-Kai Chen*[a], *Hui-Ling Liu**[a], *Xu-Ri Huang**[a]

[a] State Key Laboratory of Theoretical and Computational Chemistry, Institute of Theoretical Chemistry, Jilin University, Changchun, China, 130023.

*E-mail: huiling@jlu.edu.cn (H.-L. L.); huangxr@jlu.edu.cn (X.-R. H.)

Abstract

Developing efficient dehydrogenation is critical to understanding organic hydride hydrogen storage. The catalytic mechanism of the pH-dependent acceptorless-alcohol-dehydrogenation in aqueous solution catalyzed by a novel [C, N] cyclometalated Cp*Ir-complex, $[Ir^{III}(Cp^*)$-(4-(1*H*-pyrazol-1-yl-κN^2)benzoic acid-κC^3)$(H_2O)]_2SO_4$, has been investigated by density functional theory (DFT) with M06 dispersion-corrected functional. Using water as the solvent with liberation of dihydrogen represents a safe and clean process for such oxidations. The overall catalytic cycle has been fully characterized. The pre-catalyst $\mathbf{A_{Ir}}$ firstly reacts with the ethanol in basic solution to generate an active hydride complex $\mathbf{D_{Ir}}$ via an inner-sphere mechanism, involving the hemi-decoordination of [C, N] ligand followed by the β-H elimination. Subsequently, the complex $\mathbf{D_{Ir}}$ interacts with the protons in acid solution to generate H_2 molecule, which is a downhill process nearly

without energy barrier. The present theoretical results have shown that both the hydroxyl in basic solution and the proton in acidic solution play a crucial role in promoting the whole catalytic cycle. Therefore, our results theoretically demonstrated a significant dependence of the reaction system studied on pH value. The present study also predicted that the $\mathbf{F_{Ir}}$ (at the first triplet excited state, T_1) formed from $\mathbf{D_{Ir}}$ under laser excitation can catalyze the dehydrogenation of ethanol. Remarkably, the replacement of Ir by Ru may get efficient catalyst in the present system.

1. Introduction

Hydrogen as clean, efficient and inexhaustible energy is crucial for any clean energy policy.[1] This is in part a consequence of the progressive depletion of fossil fuel reserves and the continuously increasing energy demands. In addition, there exists a strong necessity to reduce the emission of green house gases. The majority of commercially produced hydrogen is generated from fossil fuel[2] (e.g., natural gas, liquid hydrocarbons, and coal) by steam reforming, which requires high temperatures (700-1200K), generating CO and CO_2 as waste products.[3] Therefore, producing hydrogen in a sustainable way from an environmentally friendly and promising renewable source of hydrogen is highly desired for the growing industrial needs. In response, the transition-metal-mediated alcohol dehydrogenation in the presence of hydrogen acceptors [4] (e.g., O_2, H_2O_2, and acetone) are performed with homogeneous catalysts due to their higher activity and selectivity compared with heterogeneous catalysts[5]. Nevertheless, employing the hydrogen acceptors goes against the atom

economic synthesis. Therefore, there has been increasing interests in developing efficient acceptorless-alcohol-dehydrogenation (AAD)[6] which owes preferable potential applications in H_2 production. Many ruthenium and rhodium catalysts capable of performing catalytic AADs to release hydrogen gas were reported.[4a, 4g, 7] The widely available ethanol [8] is proved to be unfeasible because high temperature or an intense light source is needed, even though it has been proposed as a promising renewable source of hydrogen. Therefore, developing new catalysts and understanding their catalytic mechanism is a key issue.

The explorative work on the ADD of ethanol catalyzed by $[RuH_2(N_2)(PPh_3)_3]$ was reported by Cole-Hamilton and co-workers[9]. In 2011, Beller experimental group efficiently gained hydrogen from alcohol under mild reaction conditions with a kind of pincer catalyst[10]. In 2012, Yamaguchi et al reported the water-soluble Cp*Ir catalyst bearing bipyridine ligand[11]. Nevertheless, their reaction temperature is still not as good as that by using catalyst recently reported by Fukuzumi group, [C,N] cyclometalated Ir hydride complex, $[Ir^{III}(Cp^*)$-(4-(1*H*-pyrazol-1-yl-κN^2)benzoic acid-κC^3)$(H_2O)]_2SO_4$, which can make hydrogen evolution form aliphatic alcohol at room temperature as well as in aqueous solution, a further improved reaction conditions[12]. This catalyst which works under mild conditions would possess significant industrial advantages. Therefore, it is crucial to give a detailed mechanism study theoretically.

In light of the work of Fukuzumi group,[12a] we performed a detailed computational mechanism study for this interesting catalytic system showing pH

dependence, using ethanol as model substrate. To present the reaction mechanism more easily, a simple frame graph is first shown in Scheme 1. As shown in Scheme 1, Fukuzumi group proposed that the pre-catalyst $\mathbf{A_{Ir}}$ firstly need to be reduced by aliphatic alcohols to produce the corresponding hydride complex $\mathbf{D_{Ir}}$ at room temperature in a basic aqueous solution. Subsequently, the active complex $\mathbf{D_{Ir}}$ can react with protons to generate a stoichiometric amount of hydrogen when the pH was decreased.[13] Simultaneously, it also can be transferred to a unique [C, C] cyclometalated Ir-hydride complex $\mathbf{F_{Ir}}$ through photoconversion.[14] The complex $\mathbf{F_{Ir}}$ can catalyze hydrogen evolution from ethanol in a basic aqueous solution under ambient conditions. In our present study, we first explore the formation of the key active complex $\mathbf{D_{Ir}}$ by comparing outer-sphere and inner-sphere two mechanisms.[6c, 15] Subsequently, the dihydrogen formations based on $\mathbf{D_{Ir}}$ and $\mathbf{F_{Ir}}$ are investigated, respectively. To understand the catalytic behavior of low-cost Ru in the present system and optimize the existing catalyst, as a comparison, the Ir^{III} is replaced by Ru^{II} and the corresponding reaction mechanism is also examined. Our study gives a theoretical understanding of how the highly active 'green' catalyst operate under catalytic conditions. It provides a solid ground for the practicing chemists to improve the existing catalysts and develop new catalysts, with an aim to broaden the scope of green and economical chemical synthesis.

Scheme 1. Overall catalytic scheme. The charge of each species is given in plain text for Ir and in parentheses for Ru.

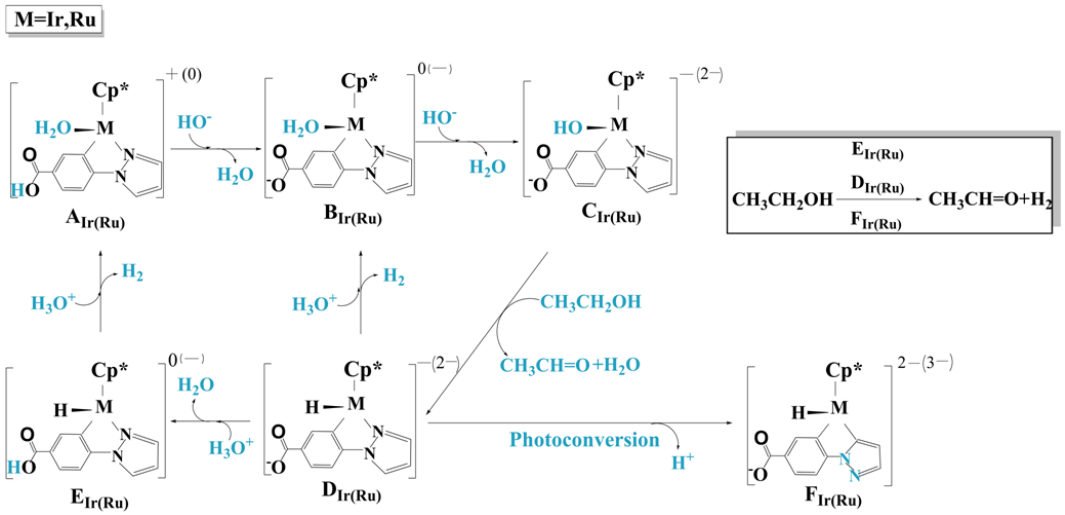

2. Computational Methods

The geometrical structures of all the species were optimized in gas phase without any geometry or symmetry constraint, using M06 [16] functional with BSI basis set (BSI represents the basis set combination of SDDALL[17] for Ir and Ru atoms and the all-electron 6-31G (d,p) for N, O, H and C atoms). The M06 functional was used due to its good predictions of both geometric parameters and reaction energies in organometallic compounds.[18] Each stationary point was classified as minima (no imaginary frequency) or transition state (only one imaginary frequency) by analytical calculation of the frequencies at the same level. In the total PESs (potential energies surface), IRC[19] (intrinsic reaction coordinate) calculation at this level was performed to confirm the correct connections among a transition state and its forward and backward minima. Based on the M06/BSI geometries, the energy of each species was refined by a single-point calculation at the M06/BSII level (BSII denotes the basis set combination of SDDALL for Ir and Ru atoms and the all-electron 6-311++G (d, p) for N, O, H and C atoms). Furthermore, the solvent correction (water solvent) was also

carried out using SMD[20] (solvation model density) continuum model, which is a universal solvation model based on the polarized continuous quantum mechanical charge density of the solute. Moreover, full vibrational and thermochemical analysis of these stationary structures were performed on optimized structures under T=298.15 K and 1 atom pressure. Because the reverse equation $H_3O^+ \rightleftharpoons H_2O+H^+$ exists in real water solution, we used the energy of H_3O^+ to calculate the protonation and deprotonation processes in the potential energy surfaces. All calculations were performed by using Gaussian 09 program package[21].

3. Results and Discussion

In this section, we describe two catalytic cycles for ethanol dehydrogenation involving the active complex $\mathbf{D_{Ir(Ru)}}$, that is, $\mathbf{A_{Ir(Ru)} \rightarrow D_{Ir(Ru)} \rightarrow A_{Ir(Ru)}}$ and $\mathbf{B_{Ir(Ru)} \rightarrow D_{Ir(Ru)} \rightarrow B_{Ir(Ru)}}$ as well as the dehydrogenation of ethanol catalyzed by $\mathbf{F_{Ir(Ru)}}$. A general schematic view is given in scheme 1. Unless otherwise mentioned, all energy values stand for the Gibbs free energy of individual reactions (ΔG) computed at the M06/BSII (SMD, water) theory level and the potential energy surfaces are located in the singlet ground state (S_0). In section 3.1, we give detailed description for ethanol dehydrogenation catalyzed by $\mathbf{A_{Ir}}$ (Figures 1-9). In section 3.2, we elucidate the analogous reaction pathways of ethanol dehydrogenation catalyzed by the newly Ru catalyst designed and the corresponding energies and structures are presented in Figures S1-S4. In section 3.3, role of H_2O molecule in H_2 generation is investigated.

3.1 The Ir model

3.1.1 The formation of the active complex D_{Ir}.

Because the saturated precursor complex $\mathbf{A_{Ir}}$ is not the active catalyst, we first investigated its activation process, that is, the transformation to the active hydride complex $\mathbf{D_{Ir}}$. The pathway description with free energy profiles are presented in Figures 1 and 3. The geometrical structures of some important stationary points selected are shown Figure 2. As shown in Figure 1, with the increase of pH value in the solution, the aqua complex $\mathbf{A_{Ir}}$ continuously releases protons from the carboxyl group and the aqua ligand to react with hydroxyl anions in basic solution, producing two water molecules. The formation of the result complex $\mathbf{C_{Ir}}$ is exothermic by 40.6 kcal/mol. Subsequently, the formation of the active complex $\mathbf{D_{Ir}}$ from $\mathbf{C_{Ir}}$ can follow either an outer-sphere mechanism (see Figure 1) or an inner-sphere mechanism (see Figure 3). In the outer-sphere mechanism, the Cp* ring is firstly slipped from η^5-coordination to η^1-coordiation, giving a vacancy at the Ir centre (intermediate **1**). This step is 16.0 kcal/mol uphill. In the intermediate **2**, one β-H of ethanol molecule interacts with the vacancy of Ir (Ir-H1, 1.86 Å), simultaneously, the hydroxyl hydride of ethanol H-bonds to the hydroxyl oxygen bonded to Ir (O1-H2, 1.58 Å). Furthermore, Ir-O1 bond (2.12 Å) between the hydroxyl ligand and Ir center is also largely weakened compared with that (1.97Å) in the intermediate **1**. Subsequently, the concerted hydrogen transfer process occurs through transition state $\mathbf{TS_{2\text{-}3}}$, that is, the β-hydride and the hydroxyl hydride of ethanol are transferred simultaneously to the vacancy of Ir and the hydroxyl ligand, respectively. The transition state $\mathbf{TS_{2\text{-}3}}$ is the highest point in overall outer-sphere pathway and is 40.7 kcal/mol much higher

relative to the stable complex $\mathbf{C_{Ir}}$ (Figure 1). In intermediate **3,** the acetaldehyde and water molecules have been fully formed. Finally, the key active complex $\mathbf{D_{Ir}}$ is easily obtained through the dissociation of water and acetaldehyde molecules coinciding with the Cp* ring returning to η^5-coordination. Our computational results show that the outer-sphere concerted mechanism involves an overall barrier as high as 40.7 kcal/mol ($\mathbf{C_{Ir}}$→$\mathbf{TS_{2\text{-}3}}$) and thus does not seem to be consistent with the room temperature experimental condition.

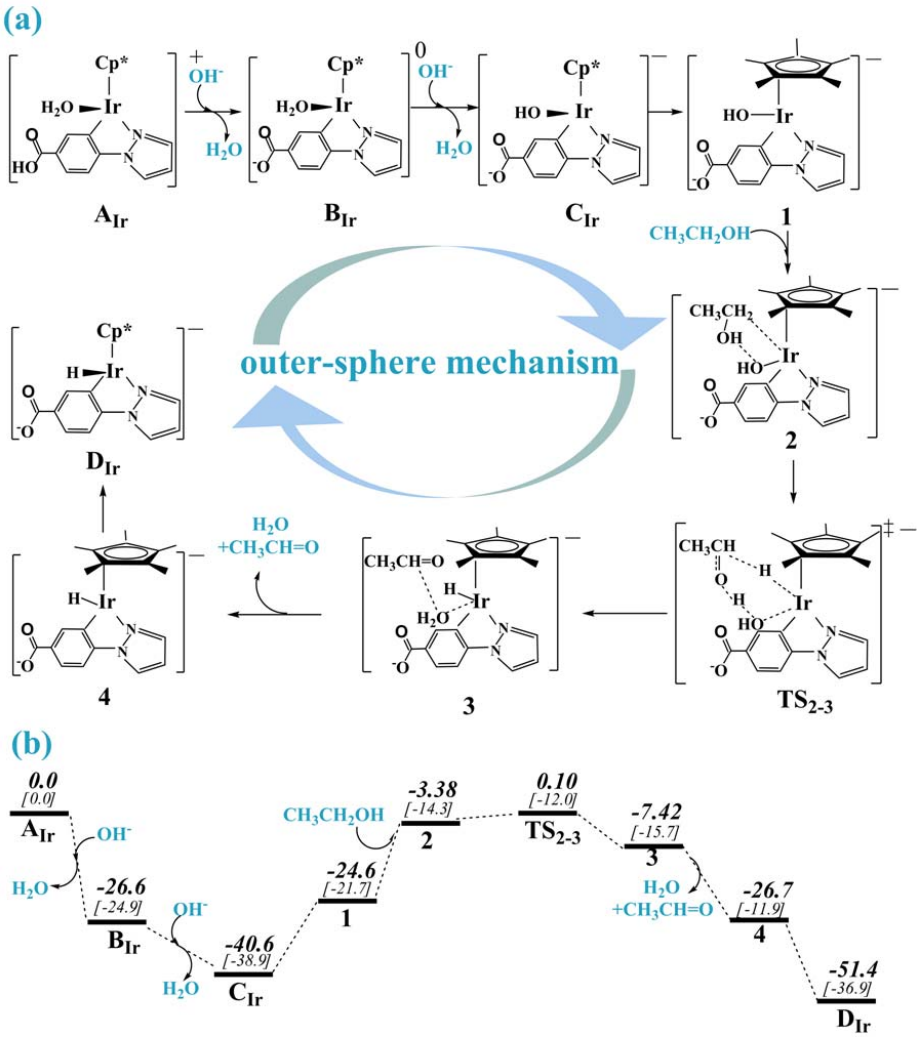

Figure 1. (a) Detailed reaction pathway of the $\mathbf{D_{Ir}}$ generation via outer-sphere mechanism; (b) the corresponding free energy profile, the values (italic numbers) are given in kcal/mol and enthalphies are listed in square brackets.

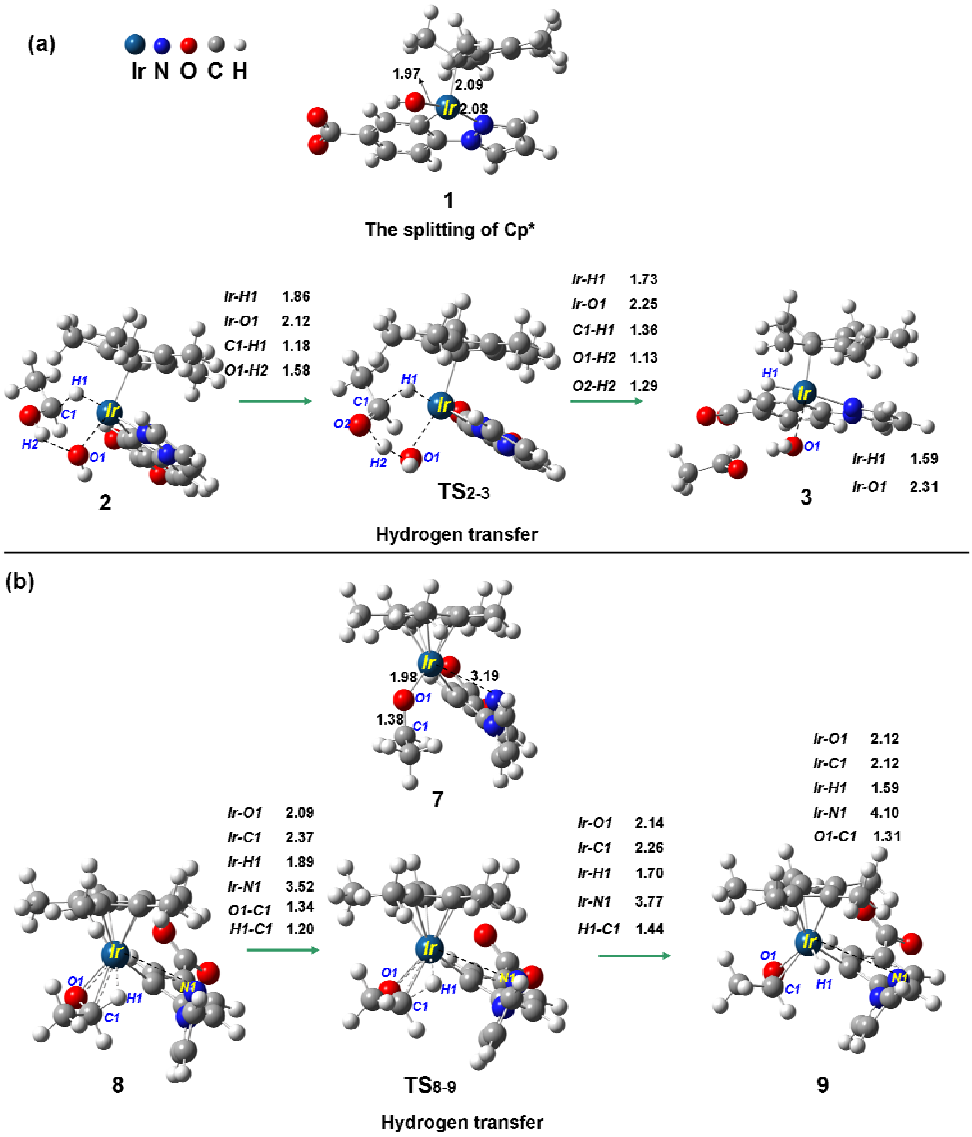

Figure 2. Geometric structures of some important stationary points selected for the formation of complex $\mathbf{D_{Ir}}$ in Figures 1 and 3 (bond length/Å).

In the inner-sphere mechanism, the coordination of ethanol to Ir takes place prior to hydrogen transfer, significant different from the outer-sphere mechanism. In intermediate **5**, the attack of the hydroxyl O atom of the ethanol on Ir leads to the decoordination of [C, N] chelated-ligand, that is, the cleavage of Ir-N bond ($d_{\text{Ir-N}}$=3.92 Å). Subsequently, the hydroxyl hydride of ethanol is transferred to the hydroxyl ligand bonded to Ir by transition state $\mathbf{TS_{5\text{-}6}}$ to afford the water in intermediate **6**. The

release of water gives the stable ethoxy intermediate **7**. The rotation of ethoxy ligand from intermediate **7** (∠Ir-O1-C1=83.6°) to **8 (**∠Ir-O1-C1=70.6°**)** plays an important role in the following *β*-hydrogen transfer to Ir, which is endothermic by 10.9 kcal/mol. Ligand rotation-promoted hydrogen transfer has also been reported in many correlative studies on ethanol dehydrogenation.[22] It is followed that the *β*-hydrogen is transferred to Ir from the CH_2 moiety of the ethoxy ligand via transition state $\mathbf{TS_{8\text{-}9}}$ ($d_{Ir\text{-}H1}$=1.70 Å and $d_{H1\text{-}C1}$=1.44 Å), leading to a hydride acetaldehyde complex **9** with a η^2-bonded acetaldehyde ligand ($d_{Ir\text{-}O1}$=2.12 Å and $d_{Ir\text{-}C1}$=2.12 Å). The process from intermediate **7** to transition state $\mathbf{TS_{8\text{-}9}}$ is climbing and endothermic by 14.6 kcal/mol. Finally, the acetaldehyde ligand is released as a free molecule in solution via transition state $\mathbf{TS_{9\text{-}10}}$ followed by a chelate ring-closing step to give the active hydride species $\mathbf{D_{Ir}}$. Herein, the release of H_2O and acetaldehyde molecules is separated, that is, a step-wise mechanism which is significant different from the above outer-sphere concerted mechanism. Our calculations show that transition states, $\mathbf{TS_{5\text{-}6}}$ (25.1 kcal/mol), $\mathbf{TS_{8\text{-}9}}$ (23.8 kcal/mol) and $\mathbf{TS_{9\text{-}10}}$ (24.0 kcal/mol) have very close energy barriers relative to $\mathbf{C_{Ir}}$. High energy of transition state $\mathbf{TS_{5\text{-}6}}$ stems from the fracture of Ir-N bond as well as the rotation of heterocyclic. The energy need for the *β*-H elimination step ($\mathbf{TS_{8\text{-}9}}$) can be ascribed to the rotation of ethoxy ligand and the Ir-H-C interaction. The high energy of transition state $\mathbf{TS_{9\text{-}10}}$ involving the acetaldehyde moving from a η^2 to η^1 coordination mode is also mentioned in alcohol dehydrogenation catalytic system reported by Michael Bühl *et al*.[23] Employing a series of the functionals M06-L, M05, and B3LYP which are usually used in

transition-metal catalytic system,[16, 18] the energies of the above three transition states relative to $\mathbf{C_{Ir}}$ are recalculated. The corresponding free energies and ethalpies are listed in Tables 1 and 2, respectively. Our results show that the same energy trend is found for all the functionals and the energies of M06-L are very similar to those of M06. Therefore, it also indicates the reliability of our computational methods used. Notice that the change of rate-determining steps between free energy and enthalpy is predicted, that is, free energy barrier ($\Delta G^{\ddagger}$) of $\mathbf{TS_{5\text{-}6}}$ and enthalpy barrier ($\Delta H^{\ddagger}$) of $\mathbf{TS_{9\text{-}10}}$ is the highest (see Tables 1 and 2, respectively). Compared to the experimental activation parameter for $\mathbf{D_{Ir}}$ formation[12a] ($\Delta H^{\ddagger}$=19.6 kcal/mol, that is, 82 kJ/mol), herein the corresponding activation parameter calculated in the M06 theory level is somewhat higher ($\mathbf{TS_{9\text{-}10}}$; $\Delta H^{\ddagger}$=23.9 kcal/mol). Furthermore, for the β-H elimination step ($\mathbf{TS_{8\text{-}9}}$) viewed as the rate-determining step for $\mathbf{D_{Ir}}$ formation in the experiment, our results demonstrate that its corresponding free energy barrier and enthalpy barrier are also high for all the functionals. Overall, the formation of $\mathbf{D_{Ir}}$ from $\mathbf{A_{Ir}}$ is thermodynamically considerable favorable (-51.3 kcal/mol) and kinetically prefer inner-sphere mechanism to outer-sphere mechanism.

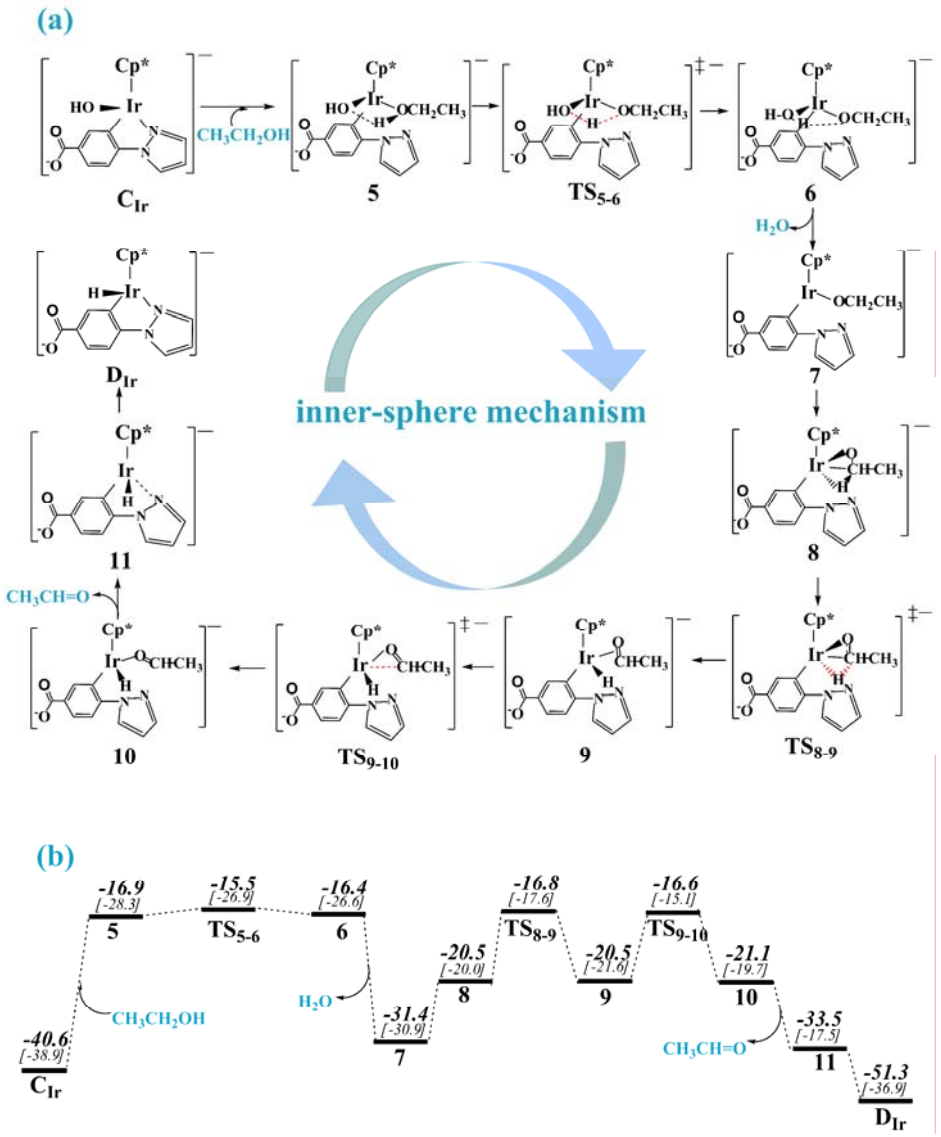

Figure 3. (a) Detailed reaction pathway of the $\mathbf{D_{Ir}}$ generation via inner-sphere mechanism; (b) the corresponding free energy profile, the values (italic numbers) are given in kcal/mol and enthalphies are listed in square brackets.

Table 1. Gibbs free energy barriers of transition states $\mathbf{TS_{5\text{-}6}}$, $\mathbf{TS_{8\text{-}9}}$ and $\mathbf{TS_{9\text{-}10}}$ relative to complex $\mathbf{C_{Ir}}$ based on M06, M06-L, and M05 and B3LYP functionals (kcal/mol).

$\Delta G^{\ddagger}$	M06	M06-L	M05	B3LYP
$\mathbf{C_{Ir}}\rightarrow\mathbf{TS_{5\text{-}6}}$	25.1	24.4	31.1	38.2
$\mathbf{C_{Ir}}\rightarrow\mathbf{TS_{8\text{-}9}}$	23.8	24.3	29.4	34.2
$\mathbf{C_{Ir}}\rightarrow\mathbf{TS_{9\text{-}10}}$	24.0	23.4	30.8	32.1

Table 2. Enthalpy barriers of transition states $\mathbf{TS_{5\text{-}6}}$, $\mathbf{TS_{8\text{-}9}}$ and $\mathbf{TS_{9\text{-}10}}$ relative to

complex $\mathbf{C_{Ir}}$ based on M06, M06-L, and M05 and B3LYP functionals (kcal/mol).

$\Delta H^{\ddagger}$	M06	M06-L	M05	B3LYP
$\mathbf{C_{Ir}}\rightarrow\mathbf{TS_{5\text{-}6}}$	10.6	11.3	18.0	25.1
$\mathbf{C_{Ir}}\rightarrow\mathbf{TS_{8\text{-}9}}$	21.3	21.9	27.0	31.7
$\mathbf{C_{Ir}}\rightarrow\mathbf{TS_{9\text{-}10}}$	23.8	23.2	30.6	31.9

3.1.2 The generation of H_2 based on $\mathbf{D_{Ir}}$ in acidic solution.

D_{Ir} and proton (H^+). The relevant reaction pathways (pathway I and II) are located in Figure 4 and the key optimized structures are shown in Figure 5. When pH value of the solution is lowered, the carboxyl anion moiety of $\mathbf{D_{Ir}}$ easily absorbs one proton from H_3O^+ to afford the complex $\mathbf{E_{Ir}'}$ in pathway I. The dissociation of the water from $\mathbf{E_{Ir}'}$ is exothermic by 6.7 kcal/mol, giving more stable complex $\mathbf{E_{Ir}}$. For the reaction of the proton with the complex $\mathbf{E_{Ir}}$ to afford H_2, two situations are considered: one is the insertion of the proton into Ir center (intermediate **12′**: $d_{\text{Ir-H1}}$=1.59 Å; $d_{\text{Ir-H2}}$ 1.59 Å); the other is a direct attach of the proton at the hydride H-Ir (intermediate **12**: $d_{\text{Ir-H1}}$=1.77 Å; $d_{\text{Ir-H2}}$ 1.78 Å; $d_{\text{H1-H2}}$=0.85 Å). As shown in Figure 4, the later case is more favorable than the former because the corresponding complex **12′** is 6.1 kcal/mol uphill compared with the complex **12**. It may be the reason that a strong nucleophilic hydritic character of the hydride H-Ir more naturally leads to its direct protonation. In addition, the steric effect around Ir also possibly hinders the insertion of the proton into Ir center. Following intermediate **12**, the decoordination of H_2 accompanied by the coordination of water molecule to Ir takes place via transition state $\mathbf{TS_{12\text{-}13}}$ ($d_{\text{H1-H2}}$=0.75 Å), leading to the intermediate **13** ($d_{\text{Ir-O}}$=2.32 Å). Finally,

the dissociation of H_2 from **13** regenerates the initial precatalyst $\mathbf{A_{Ir}}$. The above whole reaction is smoothly downhill and denoted as pathway I. Now, we turn to consider another similar pathway (II) shown in Figure 4. In this pathway, the proton directly interacts with hydride H-Ir rather than the carboxylic anion of [C, N] chelate ligand of the complex $\mathbf{D_{Ir}}$. Likewise, the intermediate **17′** analogous to **12′** is 6.5 kcal/mol unstable than intermediate **17** similar to **12**. Although the overall reaction manner of pathway II is analogous to that of pathway I, the corresponding energies are significant higher than that of pathway I, that is, the overall free energy profile of pathway II are above that of the pathway I. Therefore, we proposed that the carboxyl group of [C, N] chelate ligand enhance the catalytic activity of catalyst $\mathbf{D_{Ir}}$ for the dihydrogen formation. It also indicate the role of the proton in acidic solution in promoting the reaction proceeding. For both pathway I and II, the free energy profiles are gentle downhill and their corresponding reaction energies are acceptable in ambient reaction condition, -17.8 kcal/mol from $\mathbf{D_{Ir}}$ to $\mathbf{B_{Ir}}$ as well as -43.6 kcal/mol from $\mathbf{D_{Ir}}$ to $\mathbf{A_{Ir}}$.

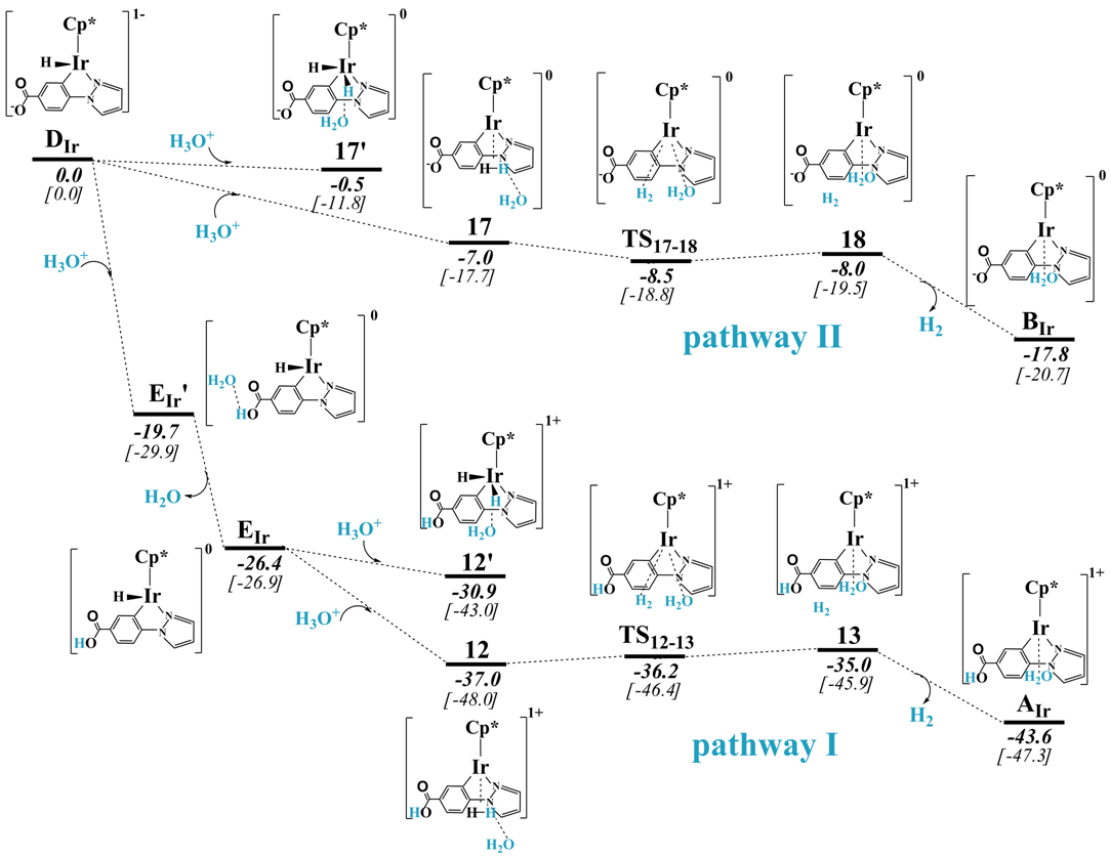

Figure 4. Detailed free energy profiles for the H_2 generation based on the complex D_{Ir} with the proton in solution. The values (italic numbers) are given in kcal/mol and enthalphies are listed in square brackets.

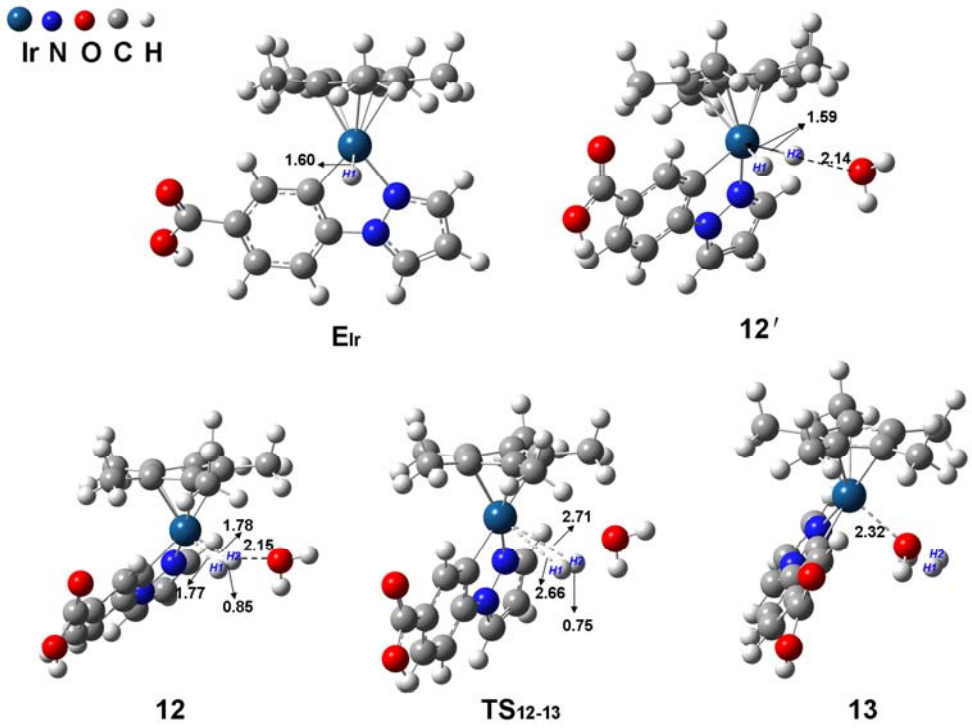

Figure 5. Geometric structures of some important stationary points selected for the generation of H_2 based on the complex $\mathbf{D_{Ir}}$ with proton presented in Figure 4 (bond length/Å).

Because the complex $\mathbf{E_{Ir}}$ is more stable than the corresponding water complex $\mathbf{E_{Ir}'}$, we consider the possible reaction pathway where the water is first dissociated from intermediate **12** or **17**. The detailed reaction manners (both pathway I and II) are shown in Figure 6. Indeed, the dissociations of the waters from **12** and **17** are exothermic by 9.4 kcal/mol and 8.0 kcal/mol to afford intermediates **14** and **19**, respectively. Subsequently, H_2 is decoordinated along flat free energy profiles (**14**→$\mathbf{TS_{14\text{-}15}}$→**15** and **19**→$\mathbf{TS_{19\text{-}20}}$→**20**). However, the last steps involving the recoordinations of water molecules to Ir centers from **16** to $\mathbf{A_{Ir}}$ and from **21** to $\mathbf{B_{Ir}}$ are endothermic by 8.0 kcal/mol and 9.3 kcal/mol, respectively. Obviously, the pathways (I and II) with a certain energy absorption in Figure 6 are kinetically unfavorable in

comparison with those in Figure 4 nearly without energy absorption.

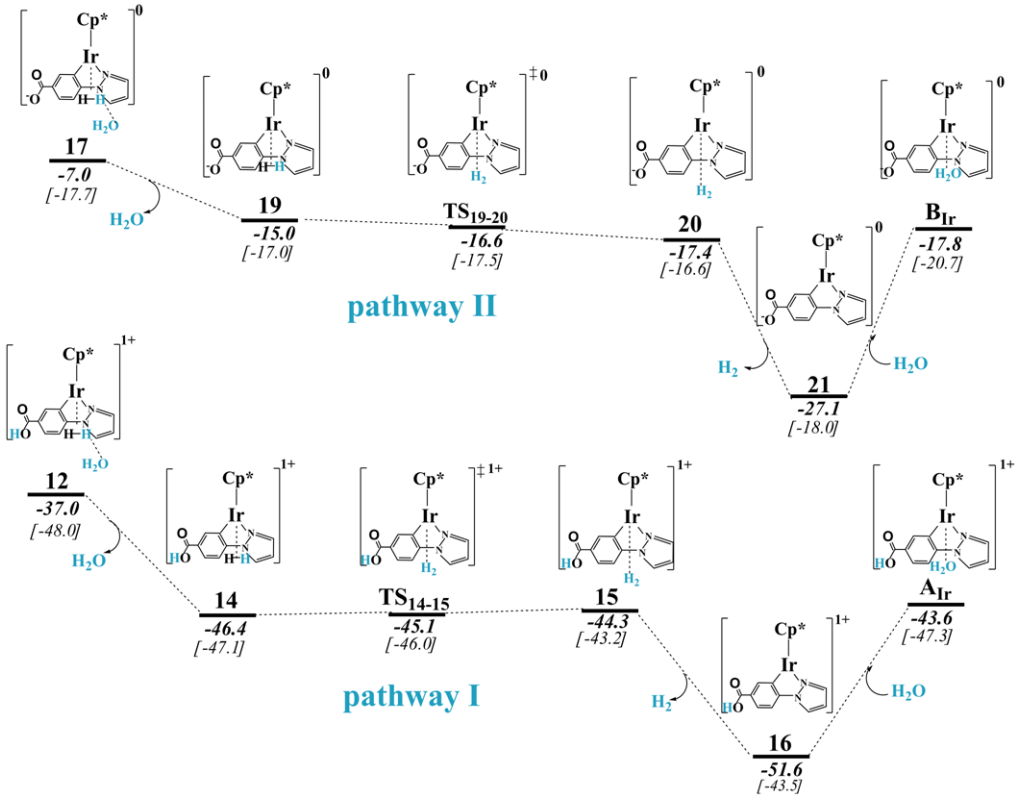

Figure 6. Detailed free energy profiles for another pathways beginning with intermediate **12** (pathway I) and **17** (pathway II), where waters are first dissociated. The values (italic numbers) are given in kcal/mol and enthalphies are listed in square brackets.

D_{Ir} and ethanol (CH_3CH_2OH). Alternatively, the ethanol molecule in solution is also a possible reactant candidate. Thus, we investigate the activity of $\mathbf{D_{Ir}}$ for ethanol dehydrogenation. The corresponding pathways (I and II) with free energies as well as the selected geometric structures are shown in Figure 7. Despite of pathway I or II, the hydroxyl hydrogen atom of ethanol first tries to approach the hydride H-Ir (intermediates **22** and **24**). Then, a six-membered transition state $\mathbf{TS_{22\text{-}23}}$ is located,

which involves the rotation of ethanol, H-H interaction between the Ir-H group and the hydroxyl hydride of ethanol. Moreover, the rotation of ethanol also leads to the Ir-H-C interaction ($d_{Ir\text{-}H3}$=2.07 Å; $d_{C\text{-}H3}$=1.19Å in **$TS_{22\text{-}23}$**). Note that very short distance between the H1 atom and H2 atom ($d_{H1\text{-}H2}$=0.84 Å in **$TS_{22\text{-}23}$**) suggests that the geometrical structure of H_2 molecule basically forms (Figure 7). These complicated interactions incur very large energy barriers, 49.8 kcal/mol for pathway I (**D_{Ir}→$TS_{22\text{-}23}$**) and 48.3 kcal/mol for pathway II (**E_{Ir}→$TS_{24\text{-}25}$**). Finally, the dissociation of H_2 and acetaldehyde completes the whole alcohol dehydrogenation reaction with +10.0 kcal/mol reaction energy. Although this reaction is a simple one-step route regardless of pathway I or II, it isn't still operative due to high energy barrier of about 49.0 kcal/mol. Therefore, for the generation of H_2 based on the complex **D_{Ir}**, the ethanol molecule should not be an appropriate reactant substrate. Overall, the proton in solution plays a crucial role in the generation of hydrogen molecule based on the complex **D_{Ir}**.

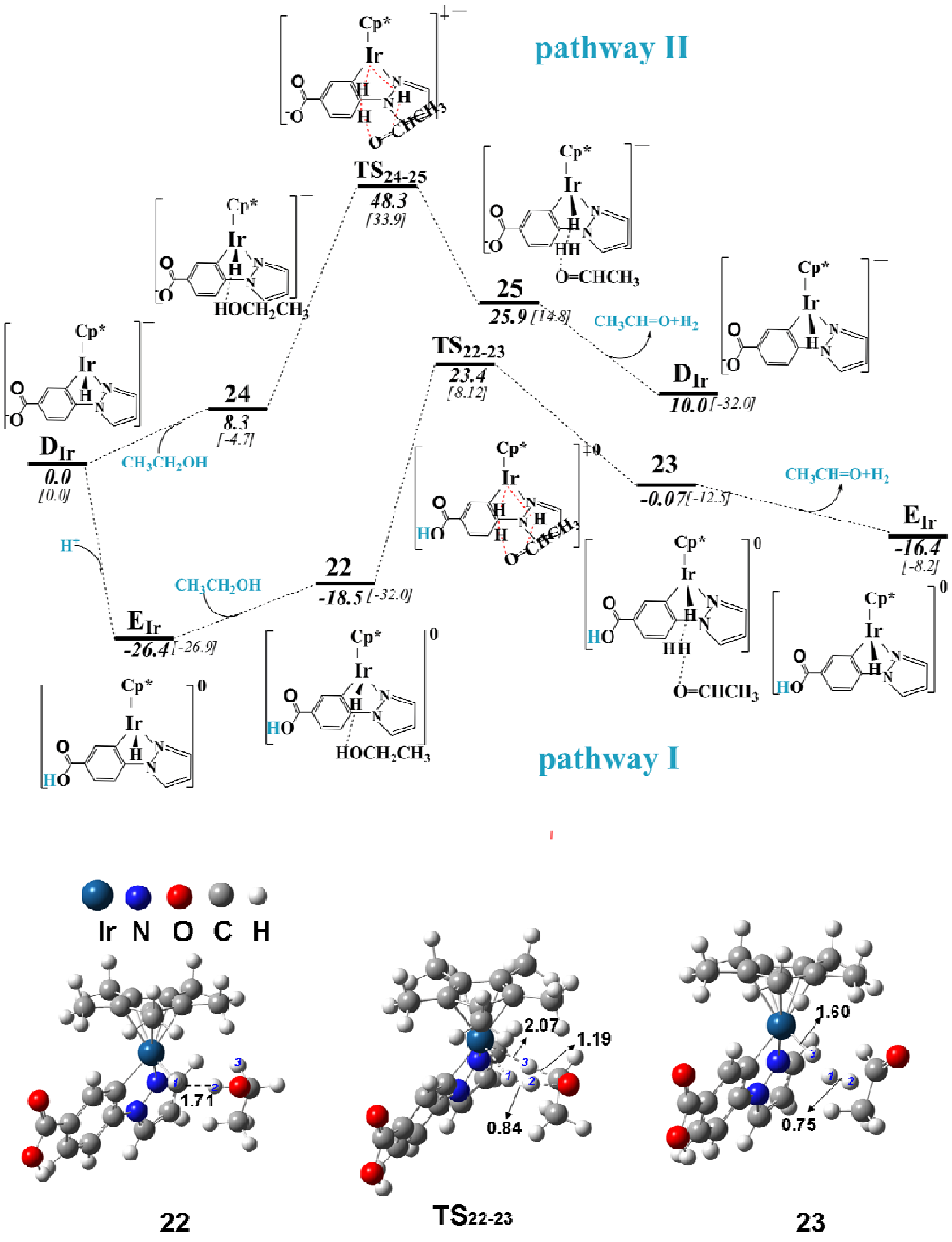

Figure 7. Detailed free energy profiles for the H_2 generation based on the complex D_{Ir} with the ethanol molecule. The values (italic numbers) are given in kcal/mol and enthalphies are listed in square brackets. Geometric structures of some important stationary points selected (bond length/Å).

Now, we summarize what happens in the catalytic cycle of the present study by combining Figure 1 (A_{Ir} to D_{Ir}) with pathway I of Figure 4 (D_{Ir} to A_{Ir}). Together, we

find two net reactions: one reaction is $C_2H_5OH \rightarrow CH_3CHO+H_2$; another reaction is $H^+ + OH^- \rightarrow H_2O$. The later one occurs twice. As shown in Figure 7, the splitting of ethanol into ethanal and H_2 is endothermic by +10.0 kcal/mol. Our DFT calculations show that the formation of water from the proton with hydroxyl is favored by -52.5 kcal/mol. The sum of three energy values, 10.0 kcal/mol, -52.5 kcal/mol and -52.5 kcal/mol, is exactly consistent with the total energy change of catalytic cycle, -95.0 kcal/mol ($\mathbf{A_{Ir}}$ to $\mathbf{D_{Ir}}$, -51.4 kcal/mol; $\mathbf{D_{Ir}}$ to $\mathbf{A_{Ir}}$, -43.6 kcal/mol). For the catalytic cycle with the carboxy anion group consisting of a part of Figure 1 ($\mathbf{B_{Ir}}$ to $\mathbf{D_{Ir}}$) and pathway II of Figure 4 ($\mathbf{D_{Ir}}$ to $\mathbf{B_{Ir}}$), the similar situation is also found. Therefore, we proposed that the reaction $H^+ + OH^- \rightarrow H_2O$ can be viewed as a driving force for promoting the catalytic cycle, which contributes to the decreasing of the total reaction energy. In addition, the reaction $H^+ + OH^- \rightarrow H_2O$ occurs in the beginning of catalytic cycle where pH value is enhanced. Therefore, our calculations intrinsically explain the reason why the reaction in the experiment takes place by tuning pH value. On one hand, through increasing pH value, the hydroxyl in aqueous solution participate in the reaction $H^+ + OH^- \rightarrow H_2O$ to promote the catalytic cycle. On the other hand, the reducing of pH value provides the protons to interact with the active hydride H-Ir of the complex $\mathbf{D_{Ir}}$ and to protonate the carboxylic anion.

3.1.3 The formation of H_2 based on F_{Ir} in base condition.

F_{Ir} and ethanol (CH_3CH_2OH). It has been reported in the experiment that the complex $\mathbf{D_{Ir}}$ can be transformed to a [C, C] cyclometalated iridium hydride complex

$\mathbf{F_{Ir}}$ under photoirradiation condition by losing one proton (see Scheme 1). On the basis of the experiment[12a], we have studied the generation of H_2 based on $\mathbf{F_{Ir}}$ with ethanol in basic condition. In the work[12a] of Fukuzumi et al, the complex $\mathbf{F_{Ir}}$ (denoted as **5** in the experiment) was formed in deaerated water containing $\mathbf{D_{Ir}}$ (denoted as **4** in the experiment) and ethanol under laser excitation at λ = 355 nm for 30min (or 50min). Because the photoconversion from $\mathbf{D_{Ir}}$ to $\mathbf{F_{Ir}}$ has been completed within 1.6 μs after laser excitation, the reaction of the complex $\mathbf{F_{Ir}}$ with ethanol is proceeding under the photoirradiation. Due to strong spin-orbital coupling effect of the transition metal Ir, it should lead to the transition from the first singlet excited state (S_1) to the first triplet exited state (T_1) via the intersystem crossing for the complex $\mathbf{F_{Ir}}$ under the photoirradiation. Therefore, the hydrogen evolution from ethanol catalyzed by $\mathbf{F_{Ir}}$ (denoted as 3-$\mathbf{F_{Ir}}$) at the first triplet exited state is studied, and the corresponding energy profile and geometric structures of some important stationary points are shown in Figure 8. The whole process can be classified into two steps: (i) the hydroxyl hydrogen of ethanol molecule interacts with the hydride H-Ir to afford the dihydrogen through transition state $\mathbf{3\text{-}TS_{1\text{-}2}}$ with an energy barrier of 20.9 kcal/mol; (ii) the *β*-H of ethanol molecule is transferred to Ir center through $\mathbf{3\text{-}TS_{3\text{-}4}}$ with an energy barrier of 8.0 kcal/mol, followed by the release of the acetaldehyde to regenerate the complex 3-$\mathbf{F_{Ir}}$. Note the highest energy barrier ($\Delta G^{\ddagger}$=20.9 kcal/mol; see Figure 8) in this process is feasible in experimental ambient condition. In addition, we also give the hydrogen evolution process from ethanol catalyzed by $\mathbf{F_{Ir}}$ at the singlet ground state (S_0), and our results indicate that its very high free energy barrier of 46.6 kcal/mol

($\mathbf{F_{Ir}}$→$\mathbf{TS_{26\text{-}27}}$) does not seem to be consistent with the room temperature experimental condition (see Figure 9). Therefore, we propose that the intersystem crossing from S_1 to T_1 under the photoexcitation may play a key role for the ethanol dehydrogenation catalyzed by $\mathbf{F_{Ir}}$.

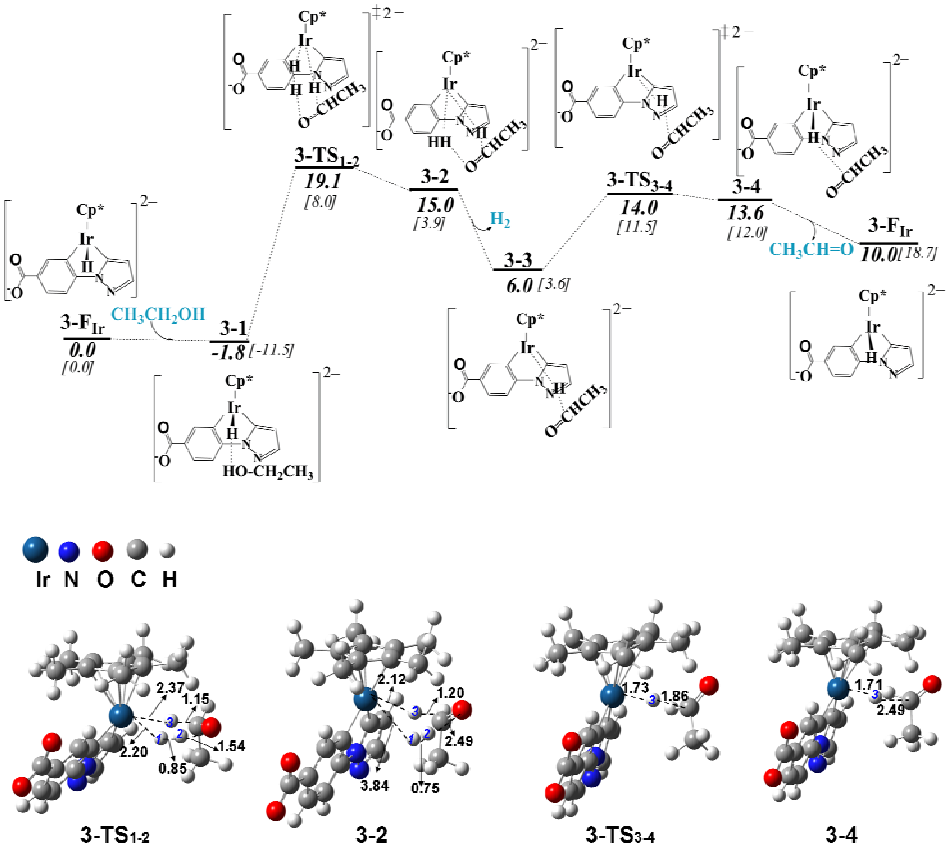

Figure 8. Detailed free energy profile for the H_2 generation based on $\mathbf{F_{Ir}}$ (expressed as 3-$\mathbf{F_{Ir}}$) at the first triplet excited state and the ethanol molecule. The values (italic numbers) are given in kcal/mol and enthalphies are listed in square brackets; Geometric structures of some important stationary points selected (bond length/Å).

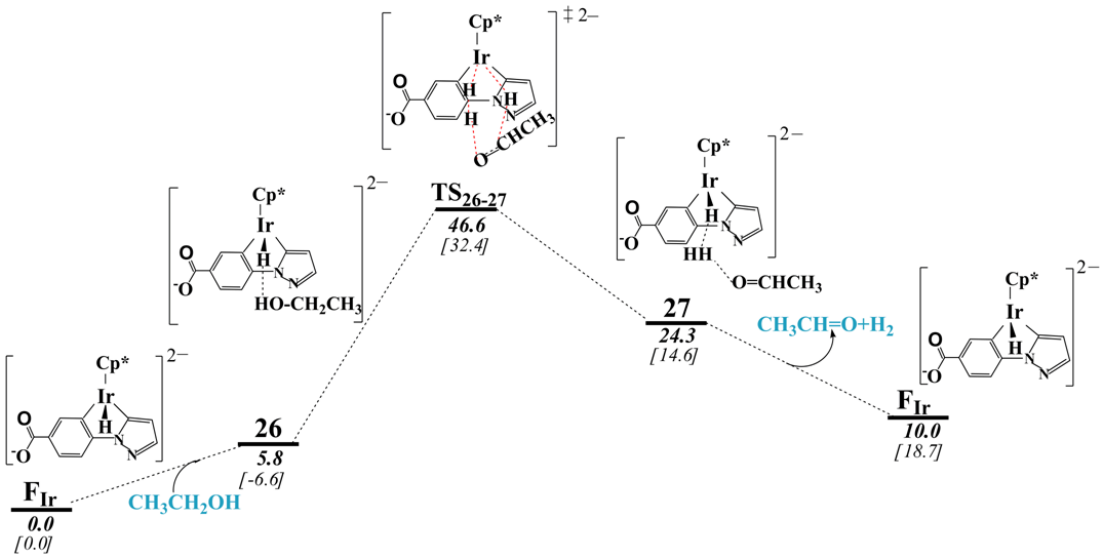

Figure 9. Detailed free energy profile of the $\mathbf{H_2}$ formation based on $\mathbf{F_{Ir}}$ at the singlet ground state and the ethanol molecule, including the free energies and enthalphies (in brackets).

3.2 The Ru model

To understand the catalytic behavior of Ru^{II} in the present system and optimize the existing catalyst, the Ir^{III} is replaced by the low-cost Ru^{II}. The corresponding energies and structures are shown in Figures S1-S5 and the same reactant substrate ethanol is used. First, the active hydride complex $\mathbf{D_{Ru}}$ is produced from $\mathbf{A_{Ru}}$ and the inner-sphere mechanism similar with that in Ir model was proposed (Figure S1). The detailed formation mechanism of $\mathbf{D_{Ru}}$ isn't discussed here because it is very similar with that of $\mathbf{D_{Ir}}$. Although herein both the free energy barrier (28.0 kcal/mol; $\mathbf{C_{Ru}} \rightarrow$ **Ru-TS$_{4\text{-}5}$**) and the reaction energy (-32.7 kcal/mol) are slightly inferior to those of $\mathbf{D_{Ir}}$ formation, these energy values still are acceptable for the $\mathbf{D_{Ru}}$ formation in experiment. Contrary to Ir catalyst system, herein H_2 generation based on $\mathbf{D_{Ru}}$ with

the proton more easily follows the pathway where water is first dissociated (Figure S3 similar to Figure 6), because the pathway involving water (Figure S2 analogous to Figure 4) needs about 10.0 kcal/mol energy absorption when the exchange between H_2O and H_2 occurs. However, the whole free energy profiles in the Figure S2 and S3 decrease by about 20 kcal/mol compared with the corresponding reactions based on $\mathbf{D_{Ir}}$, which indicates that the ruthenium complex $\mathbf{D_{Ru}}$ has the thermodynamic advantage for the reaction with the proton. Interestingly, the ethanol dehydrogenation catalyzed by active hydride complexes both $\mathbf{D_{Ru}}$ and $\mathbf{F_{Ru}}$ can take place via the step-wise mechanism, which is unacceptable in the corresponding Ir catalyst system (Figure 7 and Figure 9). Therefore, our calculations demonstrate that both $\mathbf{D_{Ru}}$ and $\mathbf{F_{Ru}}$ display better activity in the ethanol dehydrogenation. Note that herein the proton is still more possible to be the reactant compared with the ethanol molecule, which is consistent with that of Ir catalyst system. The energy gap between the highest occupied molecular orbital (HOMO) and the lowest unoccupied molecular orbital （LUMO) for a complex and its chemical reactivity have been correlated.[24] Generally, when the energy gaps are low, the reactivity is higher. Therefore, the higher reactivity of the complexes $\mathbf{D_{Ru}}$ and $\mathbf{F_{Ru}}$ should be a consequence of their much lower HOMO-LUMO energy gap (23.4 kcal/mol and 16.6 kcal/mol) compared with that (59.9 kcal/mol and 40.2 kcal/mol) for $\mathbf{D_{Ir}}$ and $\mathbf{F_{Ir}}$, respectively. Overall, the Ru catalyst $\mathbf{A_{Ru}}$ can work under mild conditions, which has significant meaning for both the experiment and industry.

3.3 Role of H_2O molecule in H_2 generation

Herein we also investigate the internal dehydrogenation of the intermediate $\mathbf{E_{Ir}}$, that is, H atom of the carboxyl group is transferred to the hydride H-Ir under the assistant of H_2O molecule (referred to as water-bridge). The corresponding energy profile and geometric structures of some important stationary points are shown in Figure 10. The corresponding transition state $\mathbf{H_2O\text{-}TS_{1\text{-}2}}$ involves a strong interaction between one $H^{\delta+}$ atom of H_2O and that $H^{\delta-}$ atom bonded to Ir, $H^{\delta+}\cdots H^{\delta-}$ (0.90 Å), accompanying with the formation of H-bond between H_2O and H atom of the carboxyl group. Although the dihydrogen is formed in the metal center of $\mathbf{H_2O\text{-}2}$, the overall reaction is endothermic by 21.0 kcal/mol with the energy barrier of 29.5 kcal/mol. Unfortunately, this water-bridge mechanism is not favorable in this catalytic system. When metal Ir is replaced by metal Ru, the same situation exists.

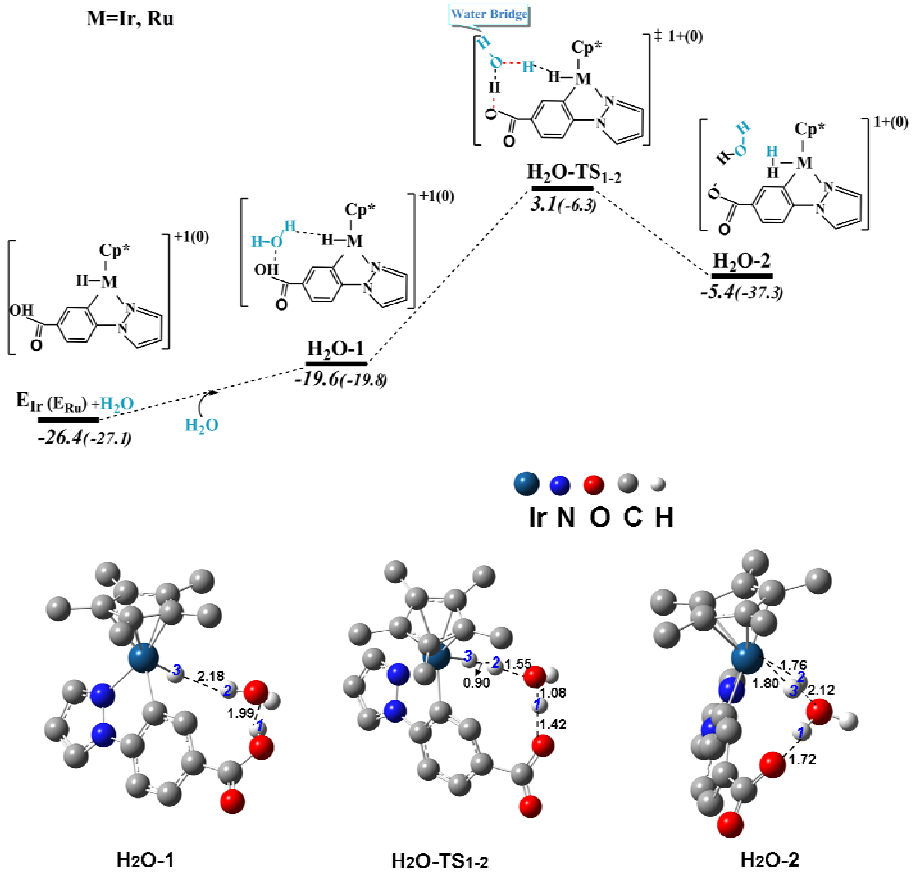

Figure 10. Free energy profile and geometric structures for the reaction involving the transfer of the carboxyl hydride to H-Ir under the assistant of H_2O molecule. The values (italic numbers) are given in kcal/mol and in parentheses for Ru. The charge of each species is given in plain text for Ir and in parentheses for Ru.

Conclusion

In summary, we have employed density functional theory to understand the mechanism of the dehydrogenative oxidation of ethanol in a pH-dependent catalytic system in aqueous solution, using a novel water-soluble Cp*Ir catalyst bearing a functional bipyridine ligand, $[Ir^{III}(Cp^*)$-(4-(1*H*-pyrazol-1-yl-κN^2)benzoic acid-κC^3)$(H_2O)]_2SO_4$. The M06 functional in combination with the SMD solvent model are used. Through increasing pH value, the reaction $H^+ + OH^- \rightarrow H_2O$ as a diving force starts the catalytic cycle. For the formation of the active complex $\mathbf{D_{Ir}}$ from $\mathbf{A_{Ir}}$, both the inner- and out-sphere mechanisms were considered, and the inner-sphere mechanism characterized by chelate ring-openning is feasible. When pH value is reduced, H_2 generation from complex $\mathbf{D_{Ir}}$ and the proton is a process without energy barrier and thus easier compared with that case with the alcohol as the reactant. Additionally, the proton can also protonate the carboxyl anion of $\mathbf{D_{Ir}}$, which is necessary for high catalytic activity. Therefore, our results have elucidated the impressive performance of catalyst in alcohol dehydrogenation by tuning pH value. In addition, for H_2 generation based on the complex $\mathbf{F_{Ir}}$ at the first triplet exited state, our results demonstrated that the highest energy barrier ($\Delta G^{\ddagger}$=20.9 kcal/mol) in this

process is feasible in experimental ambient condition. We also report that new Ru catalyst $\mathbf{A_{Ru}}$ is capable of efficient alcohol dehydrogenation under mild condition. Finally, our results indicate that the water-bridge mechanism involving the internal dehydrogenation of the intermediate $\mathbf{E_{Ir(Ru)}}$ is not favorable in this catalytic system due to its higher energy barriers. Our present study gives a theoretical understanding of how the highly active 'green' catalyst works under catalytic conditions. Moreover, it provides a solid ground for the practicing chemists to improve the existing catalysts and develop new catalysts, with an aim to broaden the scope of green and economical chemical synthesis.

Acknowledgments

This work is supported by the National Basic Research Program of China (973 Program) (2012CB932800f), the National Natural Science Foundation of China (Nos. 21303067, 21173097).

Notes and References

‡Electronic Supplementary Information (ESI) available: Detailed energy profile of $\mathbf{D_{Ru}}$ formation through inner-sphere mechanism (Figure S1); Detailed energy profiles of the H_2 formation based on the complex $\mathbf{D_{Ru}}$ and the proton (Figure S2); Detailed energy profiles for another pathway beginning with intermediate **Ru-7** (pathway I) and **Ru-9** (pathway II), where waters are firstly dissociated (Figure S3). Detailed energy profiles of the H_2 formation based on the complex $\mathbf{D_{Ru}}$ and the ethanol (Figure

S4); Detailed energy profile of the H_2 formation based on the complex $\mathbf{F_{Ru}}$ in the lowest triplet state and the ethanol molecule (Figure S5). We list the total energies and Cartesian coordinates of all the structures and the imaginary frequency of all the transition states involved in this study.

1 a) A. J. Esswein, D. G. Nocera, *Chem. Rev.* 2007**, 107**, 4022; b) S. Fukuzumi, Y. Yamada, T. Suenobu, K. Ohkubo, H. Kotani, *Energy Environ. Sci.* 2011**, 4**, 2754; c) S. Fukuzumi, *Eur. J. Inorg. Chem.* 2008**, 2008**, 1351.

2 R. M. Navarro, M. A. Peña, J. L. G. Fierro, *Chem. Rev.* 2007**, 107**, 3952.

3 a) G. W. Huber, J. W. Shabaker, J. A. Dumesic, *Science* 2003**, 300**, 2075; b) L. Huang, Q. Liu, R. Chen, A. T. Hsu, *Appl. Catal., A* 2011**, 393**, 302; c) A. Haryanto, S. Fernando, N. Murali, S. Adhikari, *Energy Fuels* 2005**, 19**, 2098.

4 a) J. V. Buijtenen, J. Meuldijk, J. A. J. M. Vekemans, L. A. Hulshof, H. Kooijman, A. L. Spek, *Organometallics* 2006**, 25**, 873; b) W. Zierkiewicz, T. Privalov, *Organometallics* 2005**, 24**, 6019; c) M. J. Schultz, R. S. Adler, W. Zierkiewicz, T. Privalov, M. S. Sigman, *J. Am. Chem. Soc.* 2005**, 127**, 8499; d) M. H. G. Prechtl, K. Wobser, N. Theyssen, Y. Ben-David, D. Milstein, W. Leitner, *Catal. Sci. Technol.* 2012**, 2**, 2039; e) T. C. Johnson, D. J. Morris, M. Wills, *Chem. Soc. Rev* 2010**, 39**, 81; f) A. M. Royer, T. B. Rauchfuss, D. L. Gray, *Organometallics* 2010**, 29**, 6763; g) J. Yuan, Y. Sun, G. A. Yu, C. Zhao, N. F. She, S. L. Mao, P. S. Huang, Z. J. Han, J. Yin, S. H. Liu, *Dalton Trans.* 2012**, 41**, 10309.

5 a) C. Pirez, M. Capron, H. Jobic, F. Dumeignil, L. Jalowiecki-Duhamel, *Angew. Chem., Int. Ed.* 2011**, 50**, 10193; b) K.-i. Shimizu, K. Kon, M. Seto, K. Shimura, H. Yamazaki, J. N. Kondo, *Green Chem.* 2013**, 15**, 418.

6 a) C. Gunanathan, D. Milstein, *Science* 2013**, 341**, 1229712; b) M. Nielsen, E. Alberico, W. Baumann, H. J. Drexler, H. Junge, S. Gladiali, M. Beller, *Nature* 2013**, 495**, 85; c) H. Li, Z. Wang, *Sci. China Chem.* 2012**, 55**, 1991; d) S. Muthaiah, S. H. Hong, *Adv. Synth. Catal.* 2012**, 354**, 3045.

7 a) K.-i. Fujita, N. Tanino, R. Yamaguchi, *Org. Lett.* 2007**, 9**, 109; b) G. R. A. Adair, J. M. J. Williams, *Tetrahedron Letters* 2005**, 46**, 8233; c) H. Junge, M. Beller, *Tetrahedron Letters* 2005**, 46**, 1031; d) H. Junge, B. Loges, M. Beller, *Chem. Commun.* 2007, 522; e) H. Nakai, S. Nakano, S. Imai, K. Isobe, *Organometallics* 2010**, 29**, 4210; f) K. Oded, S. Musa, D. Gelman, J. Blum, *Catal Commun.* 2012**, 20**, 68; g) S. Shahane, C. Fischmeister, C. Bruneau, *Catal. Sci. Technol.* 2012**, 2**, 1425.

8 a) D. Morton, D. J. Cole-Hamilton, I. D. Utuk, M. Paneque-Sosa, M. Lopez-Poveda, *Dalton Trans.* 1989, 489; b) D. Spasyuk, D. G. Gusev, *Organometallics* 2012**, 31**, 5239.

9 D. Morton, D. J. Cole-Hamilton, *Chem. Commun.* 1988, 1154.

10 M. Nielsen, A. Kammer, D. Cozzula, H. Junge, S. Gladiali, M. Beller, *Angew. Chem., Int. Ed.* 2011**, 50**, 9593.

11 R. Kawahara, K. Fujita, R. Yamaguchi, *J. Am. Chem. Soc.* 2012**, 134**, 3643.

12 a) Y. Maenaka, T. Suenobu, S. Fukuzumi, *J. Am. Chem. Soc.* 2012**, 134**, 9417; b) S. Fukuzumi, T.

Suenobu, *Dalton Trans.* 2013**, 42**, 18.

13 a) S. Ogo, K. Uehara, T. Abura, S. Fukuzumi, *J. Am. Chem. Soc.* 2004**, 126**, 3020; b) S. Ogo, K. Uehara, T. Abura, Y. Watanabe, S. Fukuzumi, *J. Am. Chem. Soc.* 2004**, 126**, 16520.

14 a) S. Fukuzumi, T. Kobayashi, T. Suenobu, *Angew. Chem., Int. Ed.* 2011**, 50**, 728; b) Y. Yamada, T. Miyahigashi, H. Kotani, K. Ohkubo, S. Fukuzumi, *J. Am. Chem. Soc.* 2011**, 133**, 16136; c) J. L. Dempsey, J. R. Winkler, H. B. Gray, *J. Am. Chem. Soc.* 2010**, 132**, 16774; d) J. L. Dempsey, J. R. Winkler, H. B. Gray, *J. Am. Chem. Soc.* 2010**, 132**, 1060.

15 a) T. Privalov, J. S. M. Samec, J. E. Bäckvall, *Organometallics* 2007**, 26**, 2840; b) J. S. Samec, J. E. Backvall, P. G. Andersson, P. Brandt, *Chem. Soc. Rev.* 2006**, 35**, 237.

16 Y. Zhao, D. G. Truhlar, *Acc. Chem. Res.* 2008**, 41**, 157.

17 D. H. Andrae, U., M. Dolg, H. Stoll, H. Preuss, *Theor. Chim. Acta.* 1990**, 77**, 123.

18 a) S. Nachimuthu, J. Gao, D. G. Truhlar, *Chem. Phys.* 2012**, 400**, 8; b) A. D. Kulkarni, D. G. Truhlar, *J. Chem. Theory Comput.* 2011**, 7**, 2325; c) Y. Zhao, D. G. Truhlar, *J. Chem. Theory Comput.* 2011**, 7**, 669; d) Y. Zhao, D. G. Truhlar, *Theor. Chem. Account.* 2007**, 120**, 215; e) C. J. Cramer, D. G. Truhlar, *Phys. Chem. Chem. Phys.* 2009**, 11**, 10757; f) R. Valero, R. Costa P. R. Moreira, D. G. Truhlar, F. Illas, *The Journal of Chemical Phisics*. 2008, **128**, 114103. g) Y. Zhao, D. G. Truhlar, *J. Chem. Theory Comput.* 2009, **5**, 325.

19 K. Fukui, *Acc. Chem. Res.* 1981**, 14**, 363.

20 A. V. Marenich, C. J. Cramer, D. G. Truhlar, *J. phys. chem. B.* 2009**, 113**, 6378.

21 Gaussian 09: M. J. Frisch, G. W. Trucks, H. B. Schlegel, G. E. Scuseria, M. A. Robb, J. R. Cheeseman, G. Scalmani, V. Barone, B. Mennucci, G. A. Peterson, H. Nakatsuji, M. Caricato, X. Li, H. P. Hratchian, A. F. Izmayl, J. Bloino, G. Zheng, J. L. Sonnenberg, M. Hada, M. Ehara, K. Toyota, R. Fukuda, J. Hasegawa, M. Ishida, T. Nakajima, Y. Honda, O. Kitao, H. Nakai, T. Vreven, J. A. Jr. Montgomery, J. E. Peralta, F. Ogliaro, M. Bearpark, J. J. Heyd, E. Brothers, K. N. Kudin, V. N. Staroverov, T. Keith, R. Kobayashi, K. Normand, K. Raghavachari, A. Rendell, J. C. Burant, S. S. Iyengar, J. Tomasi, M. Cossi, N. Rega, J. M. Millam, M. Klene, J. E. Knox, J. B. Cross, V. Bakken, C. Adamo, J. Jaramillo, R. Gomperts, R. E. Stratmann, O. Yazyev, A. J. Austin, R. Cammi, C. Pomelli, J. Ochterski, R. L. Martin, K. Morokuma, V. G. Zakrzewski, G. A. Voth, P. Salvador, J. J. Dannenberg, S. Dapprich, A. D. Daniels, O. Farkas, J. B. Foresman, J. V. Ortiz, J. Cioslowski, D. J. Fox, *GAUSSIAN 09 (Revision B.01)*, Gaussian, Inc., Wallingford, CT, 2010.

22 H. Li, J. Jiang, G. Lu, F. Huang, Z.-X. Wang, *Organometallics* 2011**, 30**, 3131.

23 N.Sieffert, M. Bühl, *J. Am. Chem. Soc.* 2010**, 132**, 8056.

24 a) R. G. Pearson, *Acc. Chem. Res.* 1993**, 26**, 250; b) P. K. Chattaraj, B. Maiti, *J. Am. Chem. Soc.* 2003**, 125**, 2705; c) F. Saleem, G. K. Rao, A. Kumar, G. Mukherjee, A. K. Singh, *Organometallics* 2013**, 32**, 3595; d) R. G. Parr, L. V. Szentpály, S. B. Liu, *J. Am. Chem. Soc.* 1999**, 121**, 1922; e) S. Liu, *J. Chem. Sci.* 2005**, 117**, 477; f) C. A. Mebi, *J. Chem. Sci.* 2011**, 123**, 727.